THE UNIVERSITY of EDINBURGH

Edinburgh Research Explorer

Mass anomalous dimension in SU(2) with two adjoint fermions

Citation for published version:
Bursa, F, Del Debbio, L, Keegan, L, Pica, C & Pickup, T 2010, 'Mass anomalous dimension in SU(2) with two adjoint fermions', *Physical Review D*, vol. 81, no. 1, 014505, pp. -.
https://doi.org/10.1103/PhysRevD.81.014505

Digital Object Identifier (DOI):
10.1103/PhysRevD.81.014505

Link:
Link to publication record in Edinburgh Research Explorer

Document Version:
Publisher's PDF, also known as Version of record

Published In:
Physical Review D

Publisher Rights Statement:
Publisher's Version/PDF: author can archive publisher's version/PDF

General rights
Copyright for the publications made accessible via the Edinburgh Research Explorer is retained by the author(s) and / or other copyright owners and it is a condition of accessing these publications that users recognise and abide by the legal requirements associated with these rights.

Take down policy
The University of Edinburgh has made every reasonable effort to ensure that Edinburgh Research Explorer content complies with UK legislation. If you believe that the public display of this file breaches copyright please contact openaccess@ed.ac.uk providing details, and we will remove access to the work immediately and investigate your claim.

OPEN ACCESS

Download date: 05. May. 2023

PHYSICAL REVIEW D **81,** 014505 (2010)

Mass anomalous dimension in SU(2) with two adjoint fermions

Francis Bursa
Jesus College, Cambridge, CB5 8BL, United Kingdom

Luigi Del Debbio, Liam Keegan, and Claudio Pica
SUPA, School of Physics and Astronomy, University of Edinburgh Edinburgh EH9 3JZ, United Kingdom

Thomas Pickup
Rudolf Peierls Centre for Theoretical Physics, University of Oxford, Oxford OX1 3NP, United Kingdom
(Received 23 October 2009; published 14 January 2010)

We study SU(2) lattice gauge theory with two flavors of Dirac fermions in the adjoint representation. We measure the running of the coupling in the Schrödinger functional scheme and find it is consistent with existing results. We discuss how systematic errors affect the evidence for an infrared fixed point (IRFP). We present the first measurement of the running of the mass in the Schrödinger functional scheme. The anomalous dimension of the chiral condensate, which is relevant for phenomenological applications, can be easily extracted from the running of the mass, under the assumption that the theory has an IRFP. At the current level of accuracy, we can estimate $0.05 < \gamma < 0.56$ at the IRFP.

DOI: 10.1103/PhysRevD.81.014505 PACS numbers: 11.15.Ha, 12.60.Nz

I. INTRODUCTION

Experiments at the LHC are about to probe nature at the TeV scale, where new physics beyond the standard model (BSM) is expected to be found. The existence of a new strongly interacting sector that is responsible for electroweak symmetry breaking is an interesting possibility. Technicolor was originally proposed 30 years ago, and strongly interacting BSM has been revisited in many instances since then. Recent reviews can be found in Refs. [1,2].

In order to be phenomenologically viable, technicolor theories need to obey the constraints from precision measurements at LEP [3,4]. Moreover the symmetry breaking needs to be communicated to the standard model, so that the usual low-energy physics is recovered. This is usually achieved in the so-called extended technicolor (ETC) models by invoking some further interaction at higher energies that couples the technicolor sector to the standard model. At the TeV scale the remnants of this coupling are higher-dimensional operators in the effective Hamiltonian, which are suppressed by powers of the high-energy scale, M, that characterizes the extended model. Among these operators are a mass term for the standard model quarks, and four-fermion interactions that would contribute to flavor-changing neutral currents (FCNC). Thus there is a tension on the possible values of M: on the one hand M needs to be large so that FCNC interactions are suppressed, on the other hand M needs to be small enough to generate the heavier quark masses. In particular, the effective operator for the standard model quark masses is

$$\mathcal{L}_m = \frac{1}{M^2}\langle\Phi\rangle\bar{\psi}\psi, \tag{1.1}$$

where ψ indicates the quark field, and Φ is the field in the technicolor theory which is responsible for electroweak symmetry breaking. In the traditional technicolor models, which are realized as SU(N) gauge theories, $\Phi = \bar{\Psi}\Psi$ is the chiral condensate of techniquarks. Let us emphasize that quark masses are defined in a given renormalization scheme and at a given scale. For instance the data reported in the Particle Data Group summaries [5] usually refer to the quark mass in the $\overline{\text{MS}}$ scheme at 2 GeV. The coefficient that appears in Eq. (1.1) is the chiral condensate at the scale M:

$$\langle\bar{\Psi}\Psi\rangle|_M = \langle\bar{\Psi}\Psi\rangle|_\Lambda \exp\left[\int_\Lambda^M \frac{d\mu}{\mu}\gamma(\mu)\right], \tag{1.2}$$

where γ is the anomalous dimension of the scalar density, and Λ is the typical scale of the technicolor theory, $\Lambda \approx 1$ TeV. The chiral condensate at this scale is expected to be $\langle\bar{\Psi}\Psi\rangle \sim \Lambda^3$, and therefore the naive expectation for the quark masses is $m \sim \Lambda^3/M^2$.

Equation (1.2) suggests a possible way to resolve the tension due to the large quark masses. If the technicolor theory is such that γ is approximately constant (and large) over a sufficiently long range in energies, then the running above will generate a power enhancement of the condensate. This scenario has been known for a long time under the name of *walking technicolor* [6–8]. Gauge theories with a large number of fermions have been traditional candidates for walking theories; the fermions slow down the running of the coupling and can potentially lead to the required power enhancement. More recent incarnations have been proposed that are constructed as SU(N) gauge theories with fermions in higher-dimensional representations of the color group [9–11]. These theories could have a genuine IR fixed point (IRFP), or simply lie in its vicinity. The existence of an IRFP is a difficult problem to address

 © 2010 The American Physical Society

since it requires to perform quantitative computations in a strongly interacting theory. Lattice simulations can provide first-principle results that can help in determining the phenomenological viability of these models; numerical simulations of models of dynamical electroweak symmetry breaking have attracted growing attention in recent years [12–40]. A number of theories have been studied: SU(3) with 8, 10, 12 flavors of fermions in the fundamental representation, SU(3) with fermions in the sextet representation, and SU(2) with fermions in the adjoint representation. These studies have focused either on the spectrum of the theories, or on the running of the coupling computed in the Schrödinger functional (SF) scheme, finding some tantalizing numerical evidence for IR behaviors different from what is known from QCD.

Existing simulations of the Schrödinger functional have identified a possible fixed point in many of the above-mentioned theories by noticing a flat behavior of the running coupling in this scheme over a given range of energy scales.

In this work we consider the SU(2) theory with two flavors of adjoint fermions, and compute the running coupling in the SF scheme. We confirm the results obtained in Ref. [32], and present a more refined analysis of the lattice data. We focus on the running of the mass in the SF scheme, from which we can extract the mass anomalous dimension that appears in Eq. (1.2). Current simulations are still plagued by systematic errors, which we examine in detail both for the coupling and the mass. These errors are the largest limitation to drawing strong conclusions from the lattice data. These limitations are common to all the studies performed so far; more extensive work is required in order to reach robust conclusions. Our results for the anomalous dimension of the mass provide crucial input for these studies that aim at exact results for nonsupersymmetric gauge theories in the nonperturbative regime.

II. SF FORMULATION

A. Basic definitions

We define the running coupling $\bar{g}^2$ nonperturbatively using the Schrödinger functional scheme [41,42]. This is defined on a hypercubic lattice of size L, with boundary conditions chosen to impose a background chromoelectric field on the system. The renormalized coupling is defined as a measure of the response of the system to a small change in the background chromoelectric field. Specifically, the spatial link matrices at $t = 0$ and $t = L$ are set, respectively, to

$$U(x, k)|_{t=0} = \exp[\eta\tau_3 a/iL], \tag{2.1}$$

$$U(x, k)|_{t=L} = \exp[(\pi - \eta)\tau_3 a/iL], \tag{2.2}$$

with $\eta = \pi/4$ [43]. The fermion fields obey

$$P_+\psi = 0, \qquad \bar{\psi}P_- = 0 \quad \text{at } t = 0, \tag{2.3}$$

$$P_-\psi = 0, \qquad \bar{\psi}P_+ = 0 \quad \text{at } t = L, \tag{2.4}$$

where the projectors are defined as $P_\pm = (1 \pm \gamma_0)/2$. The fermion fields also satisfy periodic spatial boundary conditions [44]. As we mentioned above, one can readily verify in perturbation theory that these boundary conditions impose a constant chromoelectric field.

We use the Wilson plaquette gauge action, and Wilson fermions in the adjoint representation, as implemented in Ref. [17]. Note that we have not improved the action, and therefore our results are going to be affected by $O(a)$ lattice artifacts. The same approach has been used so far for the preliminary studies of this theory in Ref. [32].

The coupling constant is defined as

$$\bar{g}^2 = k\left\langle \frac{\partial S}{\partial \eta} \right\rangle^{-1} \tag{2.5}$$

with $k = -24L^2/a^2 \sin(a^2/L^2(\pi - 2\eta))$ chosen such that $\bar{g}^2 = g_0^2$ to leading order in perturbation theory. This gives a nonperturbative definition of the coupling which depends on only one scale, the size of the system L.

To measure the running of the quark mass, we calculate the pseudoscalar density renormalization constant Z_P. Following Ref. [45], Z_P is defined by

$$Z_P(L) = \sqrt{3f_1}/f_P(L/2), \tag{2.6}$$

where f_1 and f_P are the correlation functions involving the boundary fermion fields ζ and $\bar{\zeta}$:

$$f_1 = -1/12L^6 \int d^3u d^3v d^3y d^3z \langle \bar{\zeta}'(u) \times \gamma_5\tau^a\zeta'(v)\bar{\zeta}(y)\gamma_5\tau^a\zeta(z)\rangle, \tag{2.7}$$

$$f_P(x_0) = -1/12 \int d^3y d^3z \langle \bar{\psi}(x_0)\gamma_5\tau^a\psi(x_0)\bar{\zeta}(y)\gamma_5\tau^a\zeta(z)\rangle. \tag{2.8}$$

These correlators are calculated on lattices of size L, with the spatial link matrices at $t = 0$ and $t = L$ set to unity.

The Schrödinger functional boundary conditions remove the zero modes that are normally an obstacle to simulating at zero quark mass [46]. This means we can run directly at κ_c. We determine κ_c through the PCAC mass in units of the inverse lattice spacing $am(L/2)$, where

$$am(x_0) = \frac{\frac{1}{2}(\partial_0 + \partial_0^*)f_A(x_0)}{2f_P(x_0)} \tag{2.9}$$

and

$$f_A(x_0) = -1/12 \int d^3y d^3z \langle \bar{\psi}(x_0) \times \gamma_0\gamma_5\tau^a\psi(x_0)\bar{\zeta}(y)\gamma_5\tau^a\zeta(z)\rangle. \tag{2.10}$$

Here the lattice derivatives ∂_0 and ∂_0^* are defined by $\partial_0 f(x) = f(x + 1) - f(x)$ and $\partial_0^* f(x) = f(x) - f(x - 1)$,

TABLE I. Values of β, L, κ used for the determination of $\bar{g}^2$. The entries in the table are the values of κ_c used for each combination of β and L.

β	$L=6$	$L=8$	$L=12$	$L=16$
2.00	0.190834	...	...	...
2.10	0.186174	...	...	...
2.20	0.182120	0.181447	0.1805	...
2.25	0.180514	0.179679	...	...
2.30	0.178805	0.178045	...	...
2.40	0.175480	0.174887	...	...
2.50	0.172830	0.172305	0.17172	0.17172
2.60	0.170162	0.169756	...	...
2.70	0.167706	...	...	...
2.80	0.165932	0.165550	0.16505	...
3.00	0.162320	0.162020	0.161636	0.161636
3.25	0.158505	...	0.1580	...
3.50	0.155571	0.155361	0.155132	0.155132
3.75	0.152803	...	...	...
4.00	0.150822	0.150655	...	...
4.50	0.147250	0.14720	0.14712	0.14712
8.00	0.136500	0.13645	0.136415	...

and the correlators are calculated on lattices of size L, with the spatial link matrices at $t=0$ and $t=L$ set to unity.

We define κ_c by the point where am vanishes. We measure am for 5 values of κ in the region $-0.2 < am < 0.2$ and use a linear interpolation in κ to find an estimate of κ_c. The error on κ_c is estimated by the bootstrap method.

In practice we achieve $|am| \lesssim 0.005$. We check explicitly that there is no residual sensitivity to the small remaining quark mass by repeating some of our simulations at moderately small values of $am \sim 0.02$, for which we found no shift in $\bar{g}^2$ or Z_P within the statistical uncertainty of the measured values, so the effect of our quark mass can safely be neglected.

TABLE II. Values of β, L, κ used for the determination of Z_P. The entries in the table are the values of κ_c used for each combination of β and L.

β	$L=6$	$L=8$	$L=12$	$L=16$
2.00	0.190834	...	...	...
2.05	0.188504	...	0.18625	...
2.10	0.186174	...	...	...
2.20	0.182120	0.181447	0.1805	...
2.25	0.180514	0.179679	...	...
2.30	0.178805	0.178045	...	...
2.40	...	0.174887	...	...
2.50	0.172830	0.172305	0.17172	0.17172
2.60	0.170162	0.169756	...	...
2.70	0.167706	...	...	...
2.80	0.165932	0.165550	0.16505	...
3.00	0.162320	0.162020	0.161636	0.161636
3.25	0.158505	...	0.1580	...
3.50	0.155571	0.155361	0.155132	0.155132
3.75	0.152803	...	...	...
4.00	0.150822	0.150655	0.15051	...
4.50	0.14725	0.14720	0.14712	0.14712
8.00	0.13650	0.13645	0.136415	0.136415
16.0	0.1302	0.1302	0.1302	0.130375

B. Lattice parameters

We have performed two sets of simulations in order to determine the running coupling and Z_P. The parameters of the runs are summarized, respectively, in Tables I and II. The values of κ_c are obtained from the PCAC relation as described above.

Note that Z_P is determined from a different set of runs at similar values of β, L, κ.

III. EVIDENCE FOR FIXED POINTS

Recent studies have focused on the running of the SF gauge coupling, and have highlighted a slow running in the lattice data for this quantity [13,15,31,32]. This is clearly different from the behavior observed in QCD-like theories [43,47]. These results are certainly encouraging, but have to be interpreted with care. Lattice data can single out at best a range of energies over which no running is observed. However it is not possible to conclude from lattice data only that the plateau in the running coupling does extend to arbitrarily large distances, as one would expect in the presence of a genuine IRFP. On the other hand, if the plateau has a finite extent, i.e. if the theory seems to walk only over a finite range of energies, then the behavior of the running coupling in the absence of a genuine fixed point depends on the choice of the scheme, and therefore the conclusions become less compelling.

Let us discuss the scheme dependence of the running coupling in more detail. The quantities we are interested in are the beta function and the mass anomalous dimension:

$$\mu \frac{d}{d\mu} \bar{g}(\mu) = \beta(\bar{g}), \tag{3.1}$$

$$\mu \frac{d}{d\mu} \bar{m}(\mu) = -\gamma(\bar{g}) \bar{m}(\mu), \tag{3.2}$$

where $\bar{g}$, $\bar{m}$ are the running coupling and mass in a given (mass-independent) renormalization scheme. Note that γ in Eq. (3.2) is the anomalous dimension of the scalar density, which appears also in Eq. (1.2); γ differs from the usual mass anomalous dimension by an overall sign. Both β and γ can be computed in perturbation theory for small values of the coupling constant:

$$\beta(\bar{g}) = -\bar{g}^3[\beta_0 + \beta_1 \bar{g}^2 + \beta_2 \bar{g}^4 + O(\bar{g}^6)], \tag{3.3}$$

$$\gamma(\bar{g}) = \bar{g}^2[d_0 + d_1 \bar{g}^2 + O(\bar{g}^4)]. \tag{3.4}$$

The coefficients β_0, β_1, d_0 are scheme-independent; expressions for β_0, β_1 for fermions in arbitrary representa-

tions of the gauge group have been given in Ref. [14], while for the first coefficient of the anomalous dimension, we have

$$d_0 = \frac{6C_2(R)}{(4\pi)^2}, \tag{3.5}$$

where $C_2(R)$ is the quadratic Casimir of the fermions' color representation. In the specific case we are studying in this work $d_0 = 3/(4\pi^2)$.

Different schemes are related by finite renormalizations; the running of the couplings in going from one scheme to the other is readily obtained by computing the scale dependence with the aid of the chain rule. Let us consider a change of scheme:

$$\bar{g}' = \phi(\bar{g}, m/\mu), \tag{3.6}$$

$$\bar{m}' = \bar{m}\mathcal{F}(\bar{g}, \bar{m}/\mu). \tag{3.7}$$

We impose two conditions on ϕ: it must be invertible, and should reduce to $\phi(\bar{g}) = \bar{g} + O(\bar{g}^3)$ for small values of $\bar{g}$. Equation (3.7) encodes the fact that a massless theory remains massless in any scheme. The picture simplifies considerably if one considers only mass-independent renormalization schemes; the functions ϕ and $\mathcal{F}$ only depend on the coupling $\bar{g}$, and one finds:

$$\beta'(\bar{g}') = \beta(\bar{g})\frac{\partial}{\partial \bar{g}}\phi(\bar{g}) \tag{3.8}$$

$$\gamma'(\bar{g}') = \gamma(\bar{g}) + \beta(\bar{g})\frac{\partial}{\partial \bar{g}}\log\mathcal{F}(\bar{g}). \tag{3.9}$$

The scheme-independence of the coefficients β_0, β_1, d_0 can be obtained by expanding the functions that describe the mapping between the two schemes, ϕ and $\mathcal{F}$, in powers of $\bar{g}^2$. Equations (3.8) and (3.9) summarize the main features that we want to highlight here. The conditions we imposed on ϕ imply that $\frac{\partial}{\partial \bar{g}}\phi(\bar{g}) > 0$, i.e., asymptotic freedom cannot be undone by a change of scheme. The existence of a fixed point is clearly scheme-independent: if $\beta(\bar{g}^*) = 0$ for some value $\bar{g}^*$ of the coupling, then β' has also a zero. Note that the value of the critical coupling changes from one scheme to the other, $\bar{g}'^* = \phi(\bar{g}^*)$, however the existence of the fixed point is invariant. Similarly, the anomalous dimension is scheme-independent at a fixed point, since the second term in Eq. (3.9) vanishes there. Moreover, if the change of scheme only involves a redefinition of the coupling, but leaves the mass unchanged, then the anomalous dimension does not vary.

Unfortunately none of these conclusions holds in the absence of a fixed point. In particular, a flat behavior of the running coupling over a finite range of energies can be obtained in any theory by a suitably chosen change of scheme.

It is worth stressing here another important point concerning the numerical studies of running couplings. There are instances where the beta function of an asymptotically free theory remains numerically small. This is the case of the theory considered in this work, namely, SU(2) with two flavors of adjoint Dirac fermions, in the perturbative regime. In this case the running of the coupling is very slow from the very beginning, and this is independent of the possible existence of an IRFP at larger values of the coupling. As a consequence high numerical accuracy is needed in order to resolve a "slow" running; therefore numerical studies of potential IRFP need high statistics, and a robust control of systematics. In particular it is important to extrapolate the step-scaling functions computed on the lattice to the continuum limit, in order to eliminate lattice artifacts which could bias the analysis of the dependence of the running coupling on the scale. This is particularly relevant for the studies of potential IRFP, since lattice artifacts could more easily obscure the small running that we are trying to resolve. Some of these difficulties were already noted in Ref. [32]; current results, including the ones presented in this work, are affected by these systematics.

More extensive simulations are therefore needed in order to remove the lattice artifacts by performing a controlled extrapolation of the lattice step-scaling functions defined below in Sec. IV. The scale L at which the coupling is computed and the lattice spacing a must be well separated. This last step is a crucial ingredient in the SF scheme, since it decouples the details of the lattice discretization from the running of the couplings at the scale L that we want to determine. Asymptotically free theories are effectively described by a perturbative expansion at small distances. In this regime, the degrees of freedom are the elementary fermions and the gauge bosons, renormalized couplings can be computed in perturbation theory, and different schemes can be related by perturbative calculations. The evolution of the running coupling can be followed starting from this high-energy regime and moving towards larger distances. If the theory has an IRFP, the value of the running coupling approaches some finite limit $\bar{g}^*$ as L is increased, i.e. the running coupling *must* lie in the interval $[0, \bar{g}^*]$. Its running can be traced from the UV regime up to the limiting value, which is approached from below. Larger values of $\bar{g}$ can be obtained in a lattice simulation; however the interpretation of these points is less transparent. One possibility is that the lattice theory in some region of bare parameter space lies in the basin of attraction of some nontrivial UV fixed point where a *different* continuum theory can be defined. The running coupling would then approach the IRFP value from above. The nontrivial UV fixed point is clearly difficult to identify, thereby making the extrapolation to the continuum limit rather tricky in this case.

A more pragmatic approach could be to ignore the issue of the existence of a nontrivial UV fixed point, and simply explore the limit $L/a \gg 1$, assuming that the starting point

is the lattice theory with a cutoff, and that we are only interested in the regime where distances are large compared to the cutoff. This interpretation is prone to systematic errors due to potential $O(\Lambda a)$ term, where Λ is some physical mass scale in the theory. These terms are not necessarily small, even if the limit $a/L \to 0$ is considered. Moreover, the lack of a perturbative expansion prevents us defining the running coupling properly. The conclusion is that results for $\bar{g} > \bar{g}^*$ could be affected by nonuniversal lattice artefacts.

Studies of the running couplings in the SF scheme are a useful tool to expose the possible existence of theories that show a conformal behavior at large distances. However, the results of numerical simulations have to be interpreted with care; they are unlikely to provide conclusive evidence about the existence of a fixed point by themselves, but they can be used to check the consistency of scenarios where the long-range dynamics is dictated by an IRFP. A more convincing picture can emerge when these analyses are combined with spectral studies [17,18,30,40], or MCRG methods [37].

IV. RESULTS FOR THE COUPLING

We have measured the coupling $\bar{g}^2(\beta, L)$ for a range of β, L. Our results are reported in Table III, and plotted in Fig. 1: it is clear that the coupling is very similar for different L/a at a given value of β, and hence that it runs slowly.

In Fig. 2 we compare our results to those obtained in Ref. [32]. Our results are directly comparable since we use the same action and definition of the running coupling, and it is reassuring to see that they agree within statistical errors. The numbers reported in the figure have been obtained using completely independent codes; they constitute an important sanity check at these early stages of simulating theories beyond QCD.

TABLE III. Measured values of $\bar{g}^2$ on different volumes as a function of the bare coupling β.

β	$L = 6$	$L = 8$	$L = 12$	$L = 16$
2.00	4.237(58)	...	...	...
2.10	3.682(39)	...	...	...
2.20	3.262(31)	3.457(59)	...	...
2.25	3.125(19)	3.394(54)	...	...
2.30	3.000(25)	3.090(46)	...	...
2.40	2.813(21)	2.887(44)	...	...
2.50	2.590(20)	2.682(35)	2.751(68)	3.201(324)
2.60	2.428(16)	2.460(29)	...	...
2.70	2.268(14)	...	...	...
2.80	2.141(12)	2.218(22)	2.309(40)	...
3.00	1.922(10)	1.975(25)	1.958(32)	2.025(157)
3.25	1.694(5)	...	1.830(90)	...
3.50	1.522(4)	1.585(11)	1.626(30)	1.603(76)
3.75	1.397(3)	...	...	...
4.00	1.275(3)	1.320(7)	...	...
4.50	1.101(3)	1.128(5)	1.152(10)	1.106(64)
8.00	0.558(1)	0.567(2)	0.574(3)	...

The running of the coupling is encoded in the step-scaling function $\sigma(u, s)$ as

$$\Sigma(u, s, a/L) = \bar{g}^2(g_0, sL/a)|_{\bar{g}^2(g_0, L/a)=u}, \tag{4.1}$$

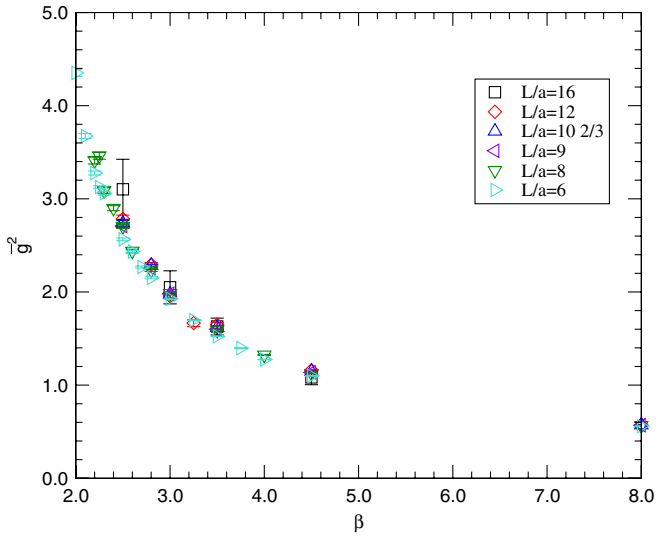

FIG. 1 (color online). Data for the running coupling as computed from lattice simulations of the Schrödinger functional. Numerical simulations are performed at several values of the bare coupling β, and for several lattice resolutions L/a. The points at $L/a = 9, 10\frac{2}{3}$ are interpolated.

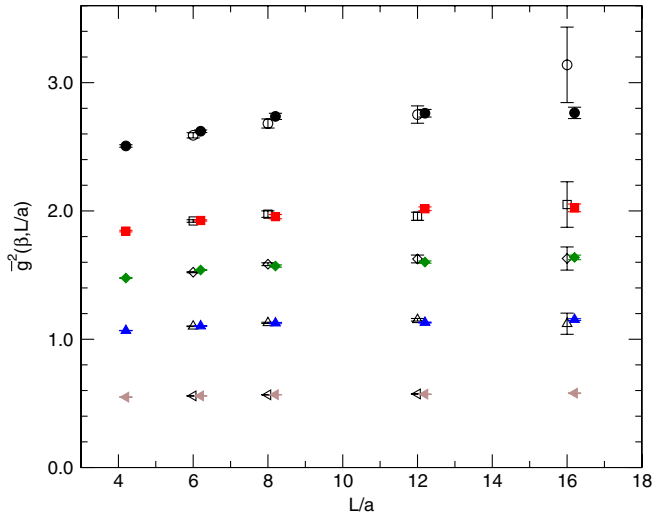

FIG. 2 (color online). The results of our numerical simulations are compared to recent results obtained in Ref. [32]. Different symbols correspond to different values of the lattice bare coupling β, corresponding, respectively, to $\beta = 2.5$, 3.0, 3.5, 4.5, 8.0. Empty symbols correspond to the data obtained in this work. Full symbols correspond to the data in Ref. [32]. Symbols have been shifted horizontally for easier reading of the plot.

$$\sigma(u, s) = \lim_{a/L \to 0} \Sigma(u, s, a/L), \tag{4.2}$$

as described in Ref. [42]. The function $\sigma(u, s)$ is the continuum extrapolation of $\Sigma(u, s, a/L)$ which is calculated at various a/L, according to the following procedure. Actual simulations have been performed at the values of β and L reported in Table I.

Starting from the actual data, we interpolate quadratically in a/L to find values of $\bar{g}^2(\beta, L)$ at $L = 9, 10\frac{2}{3}$, so that we obtain data for four steps of size $s = 4/3$ for $L \to sL$: $L = 6, 8, 9, 12$; $sL = 8, 10\frac{2}{3}, 12, 16$. Then for each L we perform an interpolation in β using the same functional form as Ref. [31]:

$$\frac{1}{\bar{g}^2(\beta, L/a)} = \frac{\beta}{2N}\left[\sum_{i=0}^{n} c_i \left(\frac{2N}{\beta}\right)^i\right]. \tag{4.3}$$

We choose to truncate the series with the number of parameters that minimizes the χ^2 per degree of freedom.

All the subsequent analysis is based on these interpolating functions, and does not make further use of the original data. Using the fitted function in Eq. (4.3), we compute $\Sigma(u, 4/3, a/L)$ at a number of points in the range $u \in [0.5, 3.5]$. A continuum extrapolation is then performed in a/L using these points to give a single estimate of $\sigma(u) \equiv \sigma(u, 4/3)$. Example extrapolations for three values of u are shown in Fig. 3. The $L = 6$ data were found to have large $O(a)$ artifacts, and are not used in the continuum extrapolation. The $L = 16$ data have a large statistical error, which limits their current impact on the continuum extrapolation. The sources of systematic uncertainty in our final results for $\sigma(u)$ are due to the interpolation in L and β and to the extrapolation to the continuum limit. Full details of the statistical and systematic error analysis are provided in Appendix A.

The resulting values for $\sigma(u)$ with statistical errors only can be seen as the black circles in Fig. 4. The red error bars in Fig. 4 also include systematic errors, but using only a constant continuum extrapolation. This is equivalent to the assumption that lattice artifacts are negligible in our data. A similar assumption has been used in Ref. [32], where the data at finite a/L were used directly to constrain the parameters that appear in the β function of the theory. The study of the lattice step-scaling function, and its continuum extrapolation, that we employ for this work, will ultimately allow us to obtain a full control over the systematic errors.

The step-scaling function encodes the same information as the β function. The relation between the two functions for a generic rescaling of lengths by a factor s is given by

$$-2\log s = \int_u^{\sigma(u,s)} \frac{dx}{\sqrt{x}\beta(\sqrt{x})}. \tag{4.4}$$

The step-scaling function can be computed at a given order in perturbation theory by using the analytic expression for the perturbative β function, and solving Eq. (4.4) for $\sigma(u, s)$. On the other hand, it can be seen directly from the definition of $\sigma(u, s)$ in Eq. (4.2) that an IRFP corresponds to $\sigma(u, s) = u$.

Our current values for the step-scaling function are consistent with a fixed point in the region $\bar{g}^2 \sim 2.0$–3.2, as reported in Ref. [32]. Further simulation at higher $\bar{g}^2$ is

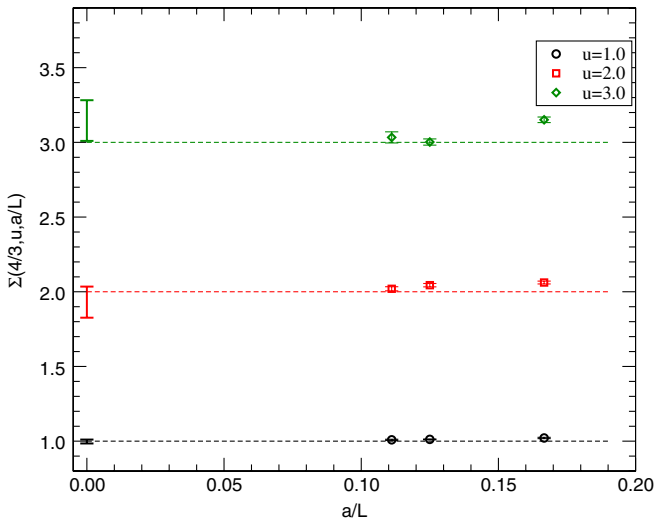

FIG. 3 (color online). Results for the lattice step-scaling function $\Sigma(4/3, u, a/L)$. The dashed lines represent the initial value of u. The point at $x = 0$ yields the value of $\sigma(u)$, i.e. the extrapolation of Σ to the continuum limit. The error bar shows the difference between constant and linear extrapolation functions, and gives an estimate of the systematic error in the extrapolation as discussed in the text.

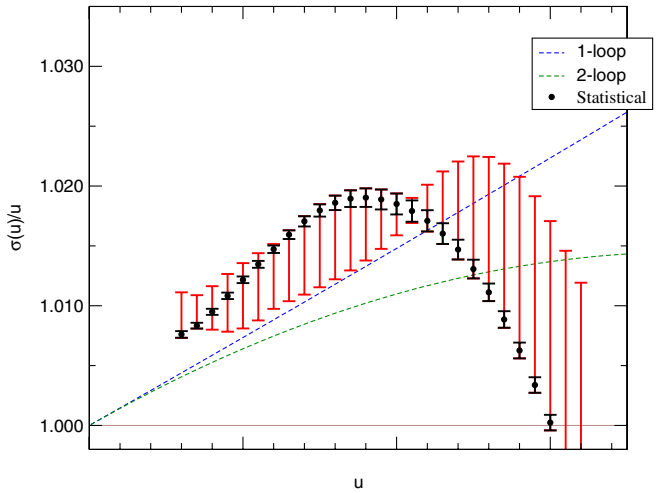

FIG. 4 (color online). The relative step-scaling function $\sigma(u)/u$ obtained after extrapolating the lattice data to the continuum limit. The black circles have a statistical error only. The red error bars also include systematic errors, but using only a constant continuum extrapolation (i.e. ignoring lattice artifacts). Note that a fixed point is identified by the condition $\sigma(u)/u = 1$.

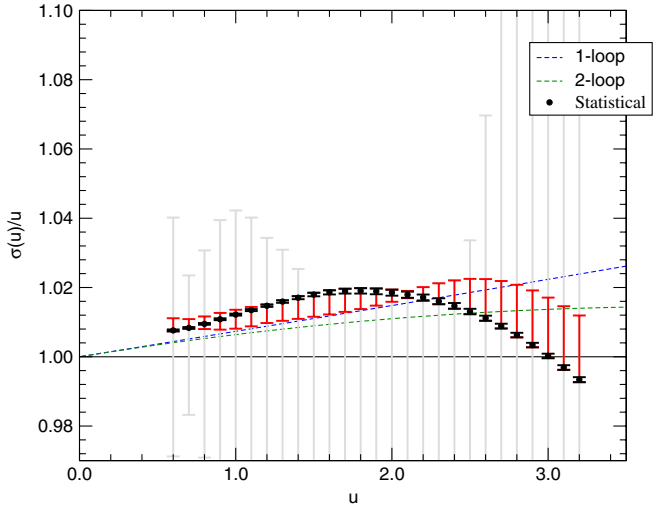

FIG. 5 (color online). The relative step-scaling function $\sigma(u)/u$ obtained after extrapolating the lattice data to the continuum limit. The black circles have a statistical error only; the red error bars include systematic errors but using only a constant continuum extrapolation; and the grey error bars give an idea of the total error by including both constant and linear continuum extrapolations.

limited by the bulk transition observed in Refs. [18,30] at $\beta \simeq 2.0$.

The errors from also including the linear continuum extrapolation are much larger and mask any evidence for a fixed point, as shown in Fig. 5. This should be a conservative estimate of the total uncertainty on $\sigma(u)$, which is dominated by systematic errors.

V. RUNNING MASS

The running of the fermion mass is determined by the scale-dependence of the renormalization constant for the pseudoscalar fermion bilinear Z_P defined in Eq. (2.6). Note that Z_P is both scheme and scale dependent. The same step-scaling technique described for the gauge coupling can be used to follow the nonperturbative evolution of the fermion mass in the SF scheme. In this work, we follow closely the procedure outlined in Ref. [48].

We have measured the pseudoscalar density renormalization constant $Z_P(\beta, L)$ for a range of β, L. Our results are reported in Table IV, and plotted in Fig. 6, where we see that there is a clear trend in Z_P as a function of L at all values of β.

The lattice step-scaling function for the mass is defined as

$$\Sigma_P(u, s, a/L) = \left.\frac{Z_P(g_0, sL/a)}{Z_P(g_0, L/a)}\right|_{\bar{g}^2(L)=u}; \qquad (5.1)$$

the mass step-scaling function in the continuum limit, $\sigma_P(u, s)$, is given by

TABLE IV. Measured values of Z_P on different volumes as a function of the bare coupling β.

β	$L = 6$	$L = 8$	$L = 12$	$L = 16$
2.00	0.3016(6)	...	...	...
2.05	0.3265(11)	...	0.2466(6)	...
2.10	0.3469(6)	...	...	...
2.20	0.3845(6)	0.3550(7)	0.3087(6)	...
2.25	0.4028(6)	0.3707(7)	...	...
2.30	0.4203(6)	0.3841(7)	...	...
2.40	...	0.4134(7)	...	...
2.50	0.4762(6)	0.4406(9)	0.3970(7)	0.3763(39)
2.60	0.5012(7)	0.4624(7)	...	...
2.70	0.5228(6)	...	...	...
2.80	0.5424(7)	0.5025(6)	0.4639(6)	...
3.00	0.5770(7)	0.5381(7)	0.5008(8)	0.4647(55)
3.25	0.6120(6)	...	0.5342(30)	0.5063(44)
3.50	0.6385(7)	0.6030(7)	0.5580(10)	0.5523(43)
3.75	0.6654(6)	...	...	...
4.00	0.6830(6)	0.6501(6)	0.6197(14)	...
4.50	0.7173(7)	0.6859(6)	0.6547(4)	0.6341(27)
8.00	0.8261(3)	0.8114(3)	0.7956(2)	0.7827(11)
16.0	0.9146(4)	0.9082(2)	0.9005(5)	0.8887(15)

$$\sigma_P(u, s) = \lim_{a\to 0} \Sigma_P(u, s, a/L). \qquad (5.2)$$

The method for calculating $\sigma_P(u) \equiv \sigma_P(u, 4/3)$ is similar to that outlined in Sec. IV for calculating $\sigma(u)$. Interpolation in β is accomplished using a function of the form:

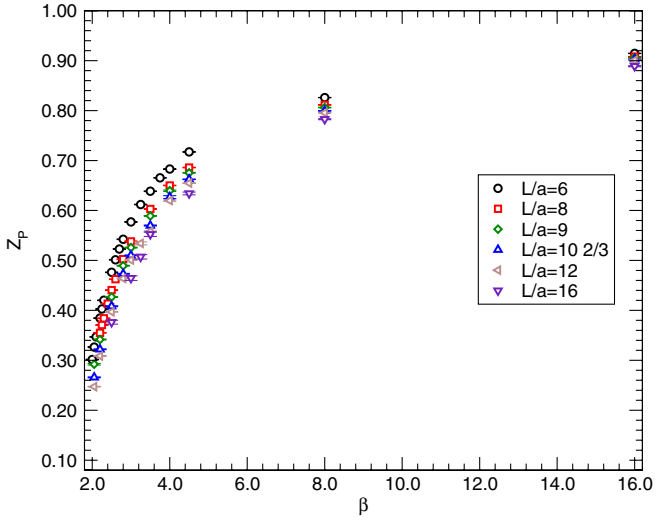

FIG. 6 (color online). Data for the renormalization constant Z_P as computed from lattice simulations of the Schrödinger functional. Numerical simulations are performed at several values of the bare coupling β, and for several lattice resolutions L/a. The points at $L/a = 9, 10\frac{2}{3}$ are interpolated.

$$Z_P(\beta, L/a) = \sum_{i=0}^{n} c_i \left(\frac{1}{\beta}\right)^i. \tag{5.3}$$

Full details of the procedure are given in Appendix B. Again the errors are dominated by systematics, in particular, the choice of continuum extrapolation function. In Fig. 7 we see that, unlike $\bar{g}^2$, Z_P has a significant variation with a/L that is fit well by a linear continuum extrapolation. The constant extrapolation is only used to quantify the errors in extrapolation.

Using the fact that $\sigma_P(u, s) = \bar{m}(\mu)/\bar{m}(\mu/s)$ for $\mu = 1/L$, we can perform an iterative step-scaling of the coupling and the mass to determine the running of the mass with scale. However, since we observe no running of the coupling within errors this is not particularly interesting.

The mass step-scaling function is related to the mass anomalous dimension (see, e.g., Ref. [48]):

$$\sigma_P(u) = \left(\frac{u}{\sigma(u)}\right)^{(d_0/(2\beta_0))} \exp\left[\int_{\sqrt{u}}^{\sqrt{\sigma(u)}} dx \left(\frac{\gamma(x)}{\beta(x)} - \frac{d_0}{\beta_0 x}\right)\right]. \tag{5.4}$$

We find good agreement with the 1-loop perturbative prediction, as shown in Fig. 8.

In the vicinity of an IRFP the relation between σ_P and γ simplifies. Denoting by γ^* the value of the anomalous dimension at the IRFP, we obtain

$$\int_{\bar{m}(\mu)}^{\bar{m}(\mu/s)} \frac{dm}{m} = -\gamma^* \int_{\mu}^{\mu/s} \frac{dq}{q}, \tag{5.5}$$

and hence

$$\log|\sigma_P(s, u)| = -\gamma^* \log s. \tag{5.6}$$

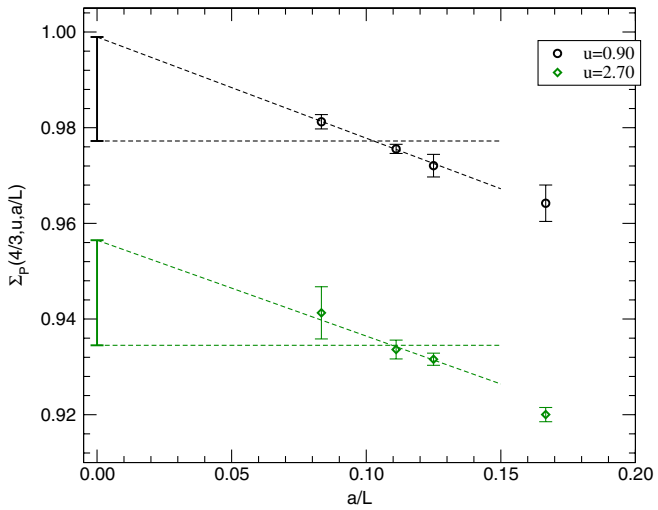

FIG. 7 (color online). Results for the lattice step-scaling function $\Sigma_P(4/3, u, a/L)$. The point at $x = 0$ yields the value of $\sigma_P(u)$, i.e. the extrapolation of Σ_P to the continuum limit. The error bar shows the difference between constant and linear extrapolation functions, and gives an estimate of the systematic error in the extrapolation as discussed in the text.

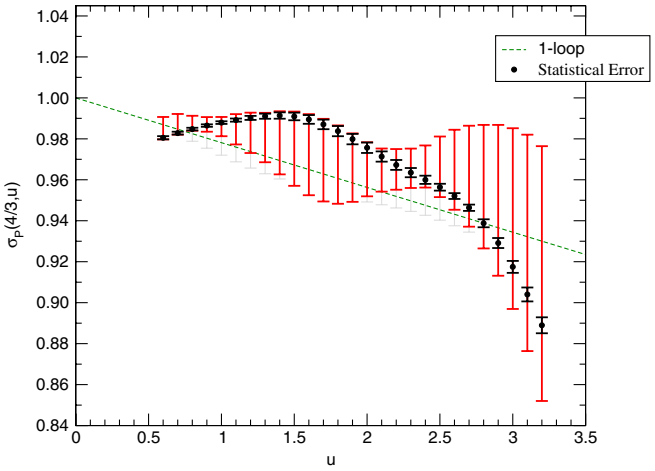

FIG. 8 (color online). The step-scaling function for the running mass $\sigma_P(u)$, using a linear continuum extrapolation. The black circles have a statistical error only; the red error bars include systematic errors using a linear continuum extrapolation. The grey error bars come from also including a constant extrapolation of the two points closest to the continuum, and give an idea of the systematic error in the continuum extrapolation.

We can therefore define an estimator

$$\hat{\gamma}(u) = -\frac{\log|\sigma_P(u, s)|}{\log|s|}, \tag{5.7}$$

which yields the value of the anomalous dimension at the fixed point. Away from the fixed point $\hat{\gamma}$ will deviate from the anomalous dimension, with the discrepancy becoming larger as the anomalous dimension develops a sizeable dependence on the energy scale.

We plot the estimator $\hat{\gamma}$ in Fig. 9. Again the error bars come from evaluating the above expression using the extremal values of $\sigma_P(u)$ at each u. We see that the actual value of $\hat{\gamma}$ is rather small over the range of interest. In particular at $\bar{g}^2 = 2.2$, the benchmark value for the IRFP tentatively found in Ref. [32], we have $\hat{\gamma} = 0.116^{+43}_{-28}$ using just the linear continuum extrapolation, and $\hat{\gamma} = 0.116^{+76}_{-28}$ if we include the constant continuum extrapolation as well. In the presence of an IRFP $\hat{\gamma}$ yields the value of the anomalous dimension, and therefore the values above can be used to bound the possible values of γ^*. The results of Ref. [32] suggest the IRFP is in the range $\bar{g}^2 = 2.0$–3.2; at the extremes of this range we find $\gamma^* = 0.086^{+85}_{-10}$ and 0.41^{+15}_{-33} using just the linear continuum extrapolation, and $\gamma^* = 0.086^{+105}_{-10}$ and 0.41^{+15}_{-33} including the constant continuum extrapolation. Over the entire range of couplings consistent with an IRFP, γ^* is constrained to lie in the range $0.05 < \gamma^* < 0.56$, even with our more conservative assessment of the continuum extrapolation errors.

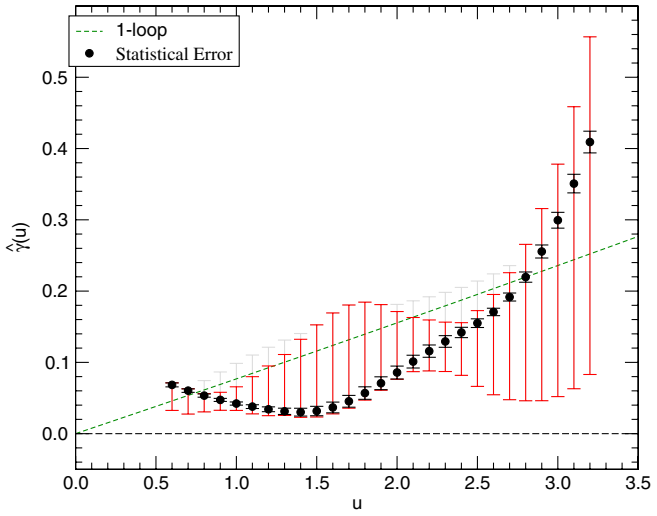

FIG. 9 (color online). The mass anomalous dimension estimator $\hat{\gamma}(u)$. The dashed line shows the 1-loop perturbative result; the black circles have a statistical error only; and the red error bars include systematic errors using a linear continuum extrapolation. The grey error bars also include a constant extrapolation of the two points closest to the continuum, giving an idea of the systematic error involved in the continuum extrapolation.

VI. CONCLUSIONS

In this paper we have presented results for the running of the Schrödinger functional coupling $\bar{g}^2$ and the mass anomalous dimension γ.

Turning first to the running of the coupling, our results are completely consistent with those of Ref. [32]. Our statistical errors are larger; however, we have carried out our analysis in a way that aims at disentangling clearly the scale dependence from the lattice artifacts. Our analysis can be systematically improved as more extensive studies are performed, and will ultimately allow us to take the continuum limit with full control over the resulting systematic errors. Our results appear to show a slowing in the running of the coupling above $\bar{g}^2 = 2$ or so, and are consistent with the presence of a fixed point where the running stops at somewhat higher $\bar{g}^2$. This is consistent with the analysis of Ref. [32]. However, once we include the systematic errors from the continuum extrapolation we find that our results no longer give any evidence for a fixed point. The fundamental reason for this is that the running of the coupling is very slow in this theory and so great accuracy is needed, in particular, near a possible fixed point.

By contrast, we find that the behavior of the anomalous dimension γ is much easier to establish. The systematic errors from the continuum extrapolation are much smaller than the signal, and we find a moderate anomalous dimension, close to the 1-loop perturbative prediction, throughout the range of β explored. In particular, in the range $\bar{g}^2 = 2.0$–3.2, where there may be an infrared fixed point, we find $0.05 < \gamma < 0.56$. These values are much smaller than those required for phenomenology, which are typically of order 1–2. Such large values of γ are clearly inconsistent with our results. The anomalous dimension at the fixed point can be computed analytically using the all-order beta function proposed in Ref. [49]. The result can be expressed as a function of group-theoretical factors only. Using the conventions described in the appendix of Ref. [14] for these group-theoretical factors, the result in Ref. [49] yields $\gamma = 3/4$, which is not too far from the bound we quote above. Given the uncertainty in the exact value of the SF coupling at the fixed point, $\gamma = 3/4$ is not strongly excluded by our current data. More precise investigations are needed to clarify this point.

The anomalous dimension is easier to measure than the beta function in candidate walking technicolor theories since it is expected to be different from zero, so we are measuring the difference of two quantities that are significantly different, say Z_P at $L = 8$ and $L = 12$. By contrast for the running of the coupling we must measure the difference of two quantities that are almost the same, since the beta function is expected to be small. Furthermore, the anomalous dimension is crucial for phenomenology; if it is not large then the presence or absence of walking behavior becomes academic. Hence the implications of our measurement of γ for the phenomenology of minimal walking technicolor call for a more precise study.

Our conclusion that γ is not large is unlikely to be affected by using larger lattices. One can see this by considering the continuum extrapolations in Fig. 7. For γ to reach, say, 1 in the continuum limit, we would need Σ_P to be $3/4 = 0.75$ at $a/L = 0$. However we see that the dependence on a/L is much too small for this to be possible, and indeed is in the wrong direction. Only a very unlikely conspiracy of lattice artifacts would make it possible for Σ_P to be as small as 0.75 in the continuum limit. On the other hand the value of $\bar{g}$ corresponding to the IRFP is currently not known with sufficient accuracy.

The results presented here are the first computation of the anomalous dimension at a putative fixed point; the systematic errors need to be reduced to make our conclusions more robust. In particular, using larger lattices would give results at smaller a/L and hence make the continuum extrapolations more accurate. It may also be necessary to use an improved action in the long term to achieve the precision required to show the existence of an IRFP or of walking behavior. However, as described above, this is very unlikely to affect our phenomenologically most important result, namely, that γ is not large. Recent results in Ref. [50] suggest that the anomalous dimension can be computed using finite-size scaling techniques. A comparison of different techniques will improve the determination of the anomalous dimension.

ACKNOWLEDGMENTS

We thank Ari Hietanen, Kari Rummukainen, and Kimmo Tuominen for useful discussions, and for providing access to their data. We also thank Francesco Sannino for discussions on the anomalous dimension at an IRFP. This work has made use of the Darwin Supercomputer of the University of Cambridge High Performance Computing Service (http://www.hpc.cam.ac.uk/), provided by Dell Inc. using Strategic Research Infrastructure Funding from the Higher Education Funding Council for England; resources funded by the University of Oxford and EPSRC; the PC cluster at the University of Southern Denmark; resources provided by the Edinburgh Compute and Data Facility (ECDF) (http://www.ecdf.ed.ac.uk/). The ECDF is partially supported by the eDIKT initiative (http://www.e-dikt.org.uk).

APPENDIX A: COUPLING ERROR ANALYSIS

We directly measure the Schrödinger functional coupling $\bar{g}^2$ and perform multiple stages of interpolation and extrapolation to extract the continuum step-scaling function $\sigma(u) \equiv \sigma(u, 4/3)$.

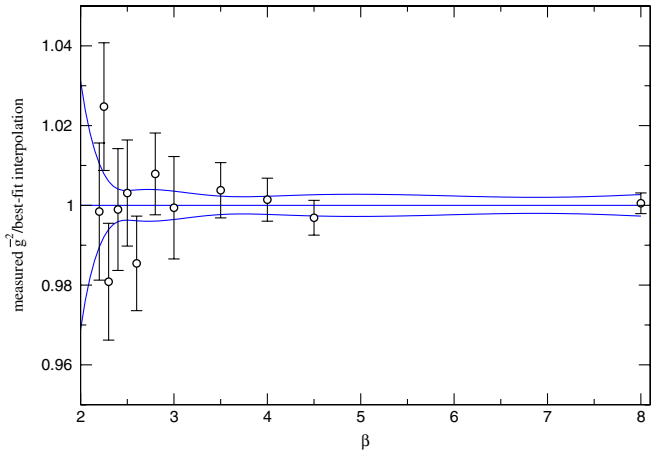

FIG. 10 (color online). Example of an interpolation function for $L = 8$, with a $\pm\sigma$ confidence interval, compared with measured $\bar{g}^2$ data points.

In order to estimate our errors for each of these stages we perform multiple bootstraps of the data. The full procedure to get a single estimate of $\sigma(u)$ can be summarized as follows:

(i) Generate $N_b \times N_a$ bootstrapped ensembles of the data and extract mean and error for each.
(ii) For each bootstrap, interpolate in a/L to find values at $L = 9, 10\frac{2}{3}$.
(iii) From each set of N_a of these find the mean and standard deviation, to give N_b interpolated data points with error bars.
(iv) For each of the N_b bootstraps do a nonlinear least squares fit for $\bar{g}^2(\beta, L)$ interpolation functions in β, an example is shown in Fig. 10.
(v) Use these functions to find N_b estimates of $\Sigma(a/L, u)$ for $L = 8$, 9, and from this extract a mean and error for each a/L.
(vi) Perform a single weighted continuum extrapolation in a/L using these points to give $\sigma(u)$.

This process is repeated N_m times, bringing the total number of bootstrap replicas of the data to $N_a \times N_b \times N_m$. This gives N_m estimates of $\sigma(u)$, from which a mean and 1-sigma confidence interval is extracted.

However, the systematic errors that result from varying the number of parameters in the interpolation functions or the continuum extrapolation functions are significantly larger than the statistical errors for the optimal set of parameters.

In order to quantify this, we repeated the entire bootstrapped process of calculating $\sigma(u)$ with a range of different interpolation and extrapolation functions, each of which gives an estimates for $\sigma(u)$, with a statistical error.

Specifically, we included two different choices for the number of parameters in the interpolating functions at each L. We kept the best fit, outlined in Table V and added the function with the second lowest χ^2 per degree of freedom as shown in Table VI. The error in the continuum extrapolation was estimated by including both constant and linear extrapolation functions. All possible combinations of these

TABLE V. Interpolation best fit parameters for $\bar{g}^2$.

$\bar{g}^2$	L/a				
	6	8	9	$10\frac{2}{3}$	12
c_0	1.409 ± 0.337	1.034 ± 0.030	0.991 ± 0.001	1.005 ± 0.001	1.001 ± 0.006
c_1	−2.043 ± 1.861	−0.355 ± 0.099	−0.215 ± 0.003	−0.259 ± 0.002	−0.257 ± 0.007
c_2	2.768 ± 4.038	0.127 ± 0.097	−0.022 ± 0.002		
c_3	−1.446 ± 4.491	−0.047 ± 0.029			
c_4	−0.253 ± 2.732				
c_5	0.457 ± 0.868				
c_6	−0.108 ± 0.113				
$\frac{\chi^2}{\text{dof}}$	2.52	2.29	1.17	2.90	3.03
dof	9	8	3	4	5

TABLE VI. Interpolation next-best fit parameters for $\bar{g}^2$.

$\bar{g}^2$	L/a				
	6	8	9	$10\frac{2}{3}$	12
c_0	1.113 ± 0.057	0.967 ± 0.050	1.010 ± 0.001	0.987 ± 0.003	0.988 ± 0.024
c_1	-0.560 ± 0.206	-0.064 ± 0.215	-0.259 ± 0.001	-0.216 ± 0.006	-0.226 ± 0.055
c_2	0.130 ± 0.216	-0.307 ± 0.328		-0.022 ± 0.003	-0.016 ± 0.028
c_3	0.366 ± 0.125	0.221 ± 0.211			
c_4	-0.136 ± 0.196	-0.059 ± 0.048			
c_5	-0.364 ± 0.234				
c_6	0.298 ± 0.127				
c_7	-0.064 ± 0.024				
$\frac{\chi^2}{\text{dof}}$	2.85	2.42	1.73	3.45	3.37
dof	8	7	4	3	4

functions gave us a set of $2^5 = 32$ values for $\sigma(u)$, each with a statistical error, which spanned the range of the systematic variation.

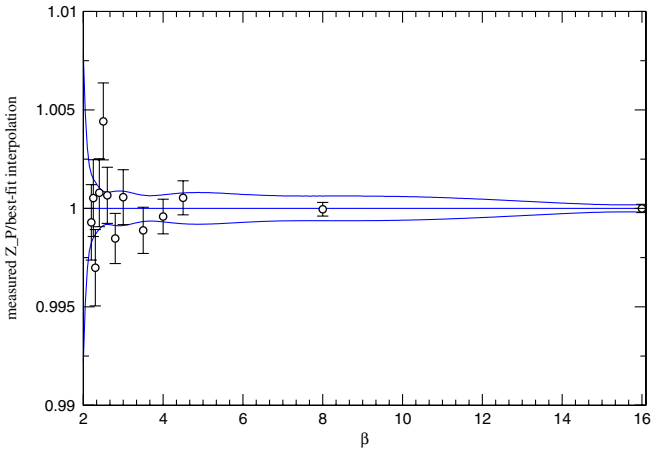

FIG. 11 (color online). Example of an interpolation function for $L = 8$, with a $\pm\sigma$ confidence interval, compared with measured Z_P data points.

For each value of u the resulting extremal values of $\sigma(u)$ were used as upper and lower bounds on the central value.

APPENDIX B: MASS ERROR ANALYSIS

The mass error analysis follows the same procedure as outlined in Appendix A with $\bar{g}^2$ replaced by Z_P. The function used to interpolate Z_P in β is given in Eq. (5.3), and an example fit is shown in Fig. 11. The c_i giving the smallest reduced χ^2 are given in Table VII and those with the second smallest in Table VIII.

In addition, Z_P converges faster than $\bar{g}^2$ and we have better 16^4 data so we can use three points in our continuum extrapolations. Again the $L = 6$ data were found to have large $O(a)$ artifacts so are not used in the continuum extrapolation, and for the constant extrapolation only the two points closest to the continuum limit are used. The fits for both $\bar{g}^2$ and Z_P are required to determine $\sigma_P(u)$, so independently varying the choice of the number of parameters for these now gives $2^{10} = 1024$ values for $\sigma_P(u)$, each with a statistical error.

TABLE VII. Interpolation best fit parameters for Z_P.

Z_P	L/a					
	6	8	9	$10\frac{2}{3}$	12	16
c_0	0.58 ± 0.30	0.93 ± 0.09	1.02 ± 0.01	1.00 ± 0.01	1.01 ± 0.01	1.01 ± 0.01
c_1	7.64 ± 6.85	-0.43 ± 1.74	-2.17 ± 0.10	-1.76 ± 0.01	-1.98 ± 0.08	-1.99 ± 0.09
c_2	-78.87 ± 60.50	-8.18 ± 12.64	4.70 ± 0.54	1.56 ± 0.05	2.30 ± 0.31	1.93 ± 0.43
c_3	361.79 ± 272.14	36.42 ± 43.33	-10.73 ± 1.27	-2.14 ± 0.06	-3.01 ± 0.34	-2.23 ± 0.64
c_4	-898.23 ± 662.83	-75.69 ± 71.04	7.96 ± 1.06			
c_5	1137.79 ± 833.32	57.07 ± 44.83				
c_6	-579.79 ± 424.25					
$\frac{\chi^2}{\text{dof}}$	2.42	1.66	2.24	4.82	6.68	6.67
dof	11	8	5	6	6	3

TABLE VIII. Interpolation next-best fit parameters for Z_P.

Z_P	L/a					
	6	8	9	$10\frac{2}{3}$	12	16
c_0	1.00 ± 0.07	1.14 ± 0.46	0.89 ± 0.02	1.00 ± 0.01	0.97 ± 0.03	0.99 ± 0.01
c_1	-1.85 ± 1.34	-5.14 ± 10.46	0.53 ± 0.40	-1.76 ± 0.14	-1.33 ± 0.46	-1.73 ± 0.03
c_2	5.09 ± 9.46	34.05 ± 93.82	-15.14 ± 2.87	1.60 ± 0.84	-1.40 ± 2.60	0.48 ± 0.08
c_3	-14.99 ± 31.38	-157.82 ± 428.42	58.03 ± 9.82	-2.22 ± 1.97	5.68 ± 6.05	
c_4	17.1 ± 49.72	405.88 ± 1059.89	-105.52 ± 15.92	0.07 ± 1.62	-7.18 ± 5.00	
c_5	-7.82 ± 30.32	-558.73 ± 1353.59	71.97 ± 9.92			
c_6		318.7 ± 700.1				
$\frac{\chi^2}{\text{dof}}$	2.46	1.75	2.32	5.97	7.47	8.03
dof	12	7	4	5	5	4

[1] Christopher T. Hill and Elizabeth H. Simmons, Phys. Rep. **381**, 235 (2003).
[2] Francesco Sannino, arXiv:0804.0182.
[3] Michael Edward Peskin and Tatsu Takeuchi, Phys. Rev. Lett. **65**, 964 (1990).
[4] Guido Altarelli and Riccardo Barbieri, Phys. Lett. B **253**, 161 (1991).
[5] C. Amsler and others (Particle Data Group), Phys. Lett. B **667**, 1 (2008), and 2009 partial update for the 2010 edition.
[6] Bob Holdom, Phys. Lett. B **150**, 301 (1985).
[7] Bob Holdom, Phys. Lett. B **143**, 227 (1984).
[8] Koichi Yamawaki, Masako Bando, and Ken-iti Matumoto, Phys. Rev. Lett. **56**, 1335 (1986).
[9] Dennis D. Dietrich and Francesco Sannino, Phys. Rev. D **75**, 085018 (2007).
[10] Roshan Foadi, Mads T. Frandsen, Thomas A. Ryttov, and Francesco Sannino, Phys. Rev. D **76**, 055005 (2007).
[11] Roshan Foadi, Mads T. Frandsen, and Francesco Sannino, Phys. Rev. D **77**, 097702 (2008).
[12] Simon Catterall and Francesco Sannino, Phys. Rev. D **76**, 034504 (2007).
[13] Thomas Appelquist, George T. Fleming, and Ethan T. Neil, Phys. Rev. Lett. **100**, 171607 (2008).
[14] Luigi Del Debbio, Mads T. Frandsen, Haralambos Panagopoulos, and Francesco Sannino, J. High Energy Phys. 06 (2008) 007.
[15] Yigal Shamir, Benjamin Svetitsky, and Thomas DeGrand, Phys. Rev. D **78**, 031502 (2008).
[16] Albert Deuzeman, Maria Paola Lombardo, and Elisabetta Pallante, Phys. Lett. B **670**, 41 (2008).
[17] Luigi Del Debbio, Agostino Patella, and Claudio Pica, arXiv:0805.2058.
[18] Simon Catterall, Joel Giedt, Francesco Sannino, and Joe Schneible, J. High Energy Phys. 11 (2008) 009.
[19] Benjamin Svetitsky, Yigal Shamir, and Thomas DeGrand, Proc. Sci., LATTICE2008 (2008) 062 [arXiv:0809.2885].
[20] Thomas DeGrand, Yigal Shamir, and Benjamin Svetitsky, Proc. Sci., LATTICE2008 (2008) 063 [arXiv:0809.295].
[21] Zoltan Fodor, Kieran Holland, Julius Kuti, Daniel Nogradi, and Chris Schroeder, Proc. Sci., LATTICE2008 (2008) 058 [arXiv:0809.4888].
[22] Zoltan Fodor, Kieran Holland, Julius Kuti, Daniel Nogradi, and Chris Schroeder, Proc. Sci., LATTICE2008 (2008) 066 [arXiv:0809.4890].
[23] Albert Deuzeman, Maria Paola Lombardo, and Elisabetta Pallante, Proc. Sci., LATTICE2008 (2008) 060 [arXiv:0810.1719].
[24] Albert Deuzeman, Elisabetta Pallante, Maria Paola Lombardo, and E. Pallante, Proc. Sci., LATTICE2008 (2008) 056 [arXiv:0810.3117].
[25] Ari Hietanen, Jarno Rantaharju, Kari Rummukainen, and Kimmo Tuominen, Proc. Sci., LATTICE2008 (2008) 065 [arXiv:0810.3722].
[26] Xiao-Yong Jin and Robert D. Mawhinney, Proc. Sci., LATTICE2008 (2008) 059 [arXiv:0812.0413].
[27] Luigi Del Debbio, Agostino Patella, and Claudio Pica, Proc. Sci., LATTICE2008 (2008) 064 [arXiv:0812.0570].
[28] Thomas DeGrand, Yigal Shamir, and Benjamin Svetitsky, Phys. Rev. D **79**, 034501 (2009).
[29] George T. Fleming, Proc. Sci., LATTICE2008 (2008) 021 [arXiv:0812.2035].
[30] Ari J. Hietanen, Jarno Rantaharju, Kari Rummukainen, and Kimmo Tuominen, J. High Energy Phys. 05 (2009) 025.
[31] Thomas Appelquist, George T. Fleming, and Ethan T. Neil, Phys. Rev. D **79**, 076010 (2009).
[32] Ari J. Hietanen, Kari Rummukainen, and Kimmo Tuominen, arXiv:0904.0864.
[33] A. Deuzeman, M. P. Lombardo, and E. Pallante, Phys. Rev. D **80**, 094504 (2009).
[34] Zoltan Fodor, Kieran Holland, Julius Kuti, Daniel Nogradi, and Chris Schroeder, J. High Energy Phys. 08 (2009) 084.
[35] Thomas DeGrand and Anna Hasenfratz, Phys. Rev. D **80**, 034506 (2009).
[36] Thomas DeGrand, arXiv:0906.4543.
[37] Anna Hasenfratz, Phys. Rev. D **80**, 034505 (2009).
[38] L. Del Debbio, B. Lucini, A. Patella, C. Pica, and A. Rago, Phys. Rev. D **80**, 074507 (2009).
[39] Zoltan Fodor, Kieran Holland, Julius Kuti, Daniel Nogradi, and Chris Schroeder, arXiv:0907.4562.
[40] C. Pica, L. Del Debbio, B. Lucini, A. Patella, and A. Rago, arXiv:0909.3178.

[41] Martin Luscher, Peter Weisz, and Ulli Wolff, Nucl. Phys. **B359**, 221 (1991).
[42] Martin Luscher, Rajamani Narayanan, Peter Weisz, and Ulli Wolff, Nucl. Phys. **B384**, 168 (1992).
[43] Martin Luscher, Rainer Sommer, Ulli Wolff, and Peter Weisz, Nucl. Phys. **B389**, 247 (1993).
[44] Stefan Sint and Rainer Sommer, Nucl. Phys. **B465**, 71 (1996).
[45] Stefano Capitani, Martin Luscher, Rainer Sommer, and Hartmut Wittig, Nucl. Phys. **B544**, 669 (1999).
[46] Stefan Sint, Nucl. Phys. **B421**, 135 (1994).
[47] Michele Della Morte *et al.*, Nucl. Phys. **B713**, 378 (2005).
[48] Michele Della Morte *et al.*, Nucl. Phys. **B729**, 117 (2005).
[49] Thomas A. Ryttov and Francesco Sannino, Phys. Rev. D **78**, 065001 (2008).
[50] Thomas DeGrand, arXiv:0910.3072.